Advanced models for the calculation of capillary attraction in axisymmetric configurations

Raffaele Ardito, Alberto Corigliano*, Attilio Frangi, Francesco Rizzini

Dept. of Civil and Environmental Engineering, Politecnico di Milano, Piazza Leonardo da Vinci 32, Milan I-20133, Italy

Received 8 October 2013
Accepted 2 May 2014
Available online 23 May 2014

1. Introduction

The reliability of Micro-Electro-Mechanical Systems (MEMS) is a topic of paramount importance for technological advances: proper design and fabrication of micro-devices must ensure the perfect functioning both in standard exercise conditions and in extreme situations. Among the various dangerous phenomena, spontaneous adhesion can seriously compromise the MEMS reliability. Due to the high surface-to-volume ratio, the adhesive forces between parts in contact may exceed the elastic restoring force: in this case, the components remain stuck to each other and the microsystem can be completely unusable. This situation is addressed to in the literature as *stiction*, a neologism coined from *static friction* (see e.g. (Mastragelo and Hsu, 1993) and (Tas et al., 2003)).

Various phenomena can contribute to the adhesion at the nanoscale causing attractive forces between components: the most relevant ones are van der Waals (Delrio et al., 2005) and capillarity forces (Hariri et al., 2007). This research mainly focuses on the latter, caused by liquid menisci capillary condensation which entails the formation of liquid menisci around the contact areas of two neighbouring asperities. The computation of the capillarity forces is subordinated to the evaluation of the shape of the meniscus and the solution of such a problem represents an awkward task. One can follow two different approaches (Payam and Fathipour, 2011) depending on whether or not thermodynamic equilibrium is assumed between the liquid and the surrounding gas. If equilibrium is assumed, the meniscus mean curvature is constant and Kelvin equation holds, which is solvable either in analytical (Stifter et al., 2000) or in numerical (Pakarinen et al., 2005, Chau et al., 2007) way; if no equilibrium is assumed, a formulation based on liquid volume conservation must be considered. Many works refer to this situation (Rabinovich et al., 2005, Mu and Su, 2007, Payam and Fathipour, 2011); however it is more realistic to assume thermodynamic equilibrium since, in a typical situation, menisci between MEMS components are caused by capillarity condensation and there is no way to evaluate the volume of the liquid bridges from which the estimate of the force depends (Butt, 2008).

Whatever option will be taken, the proper evaluation of the capillarity force requires the computation of the geometrical shape of the menisci. In spite of many important theoretical studies (see e.g. (Lian et al., 1993; Melrose, 1966)), there is a lack of general methods to be applied for obtaining the exact configuration of the liquid bridge. The problem has been tackled for simple cases, such as a meniscus between two spheres or between a sphere and a flat. As a matter of fact, those cases are consistently far away from the realistic situation of rough surface, endowed with a random distribution of asperities with generic shape. Nonetheless, it is possible to envisage that satisfactory results could be obtained by replacing the actual geometry of the asperities by means of approximate axisymmetric surfaces. In this ambit, many

* Corresponding author. Tel.: +39 0223994244.
E-mail address: alberto.corigliano@polimi.it (A. Corigliano).

approximations have been proposed, both geometric and numeric, as equal contact angle with the two particles between which the meniscus is formed (Israelachvili, 2011, Lambert et al., 2008, Mu and Su, 2007), same radius for the two spheres (Mu and Su, 2007, Rabinovich et al., 2005), circular arc or paraboloid approximation for the vertical profile of the liquid bridge interface (de Lazzer et al., 1999, Pepin et al., 2000, Stifter et al., 2000): it is demonstrated that circular approximation is suitable in many situations (Pakarinen et al., 2005). Another approximation that usually holds is based on the assumption that the liquid menisci extend much further in the direction parallel to the gap than normal to it (de Boer and de Boer, 2007, Butt, 2008), which is reasonable only when the distance between the particles is quite small. Otherwise, it can lead to a discrepancy between the calculated forces and experimental results because menisci can be stretched along their axis and the assumption does not hold anymore.

In this research, a new predictive analytical tool for the attractive force due to a single meniscus in axisymmetric conditions has been developed, with the aim of obtaining the exact solution for the meniscus shape in the hypothesis of thermodynamic equilibrium. The analytical tool has been obtained by applying, in an innovative way, a mathematical procedure originally proposed in (Kenmotsu, 1980). The results obtained by the exact approach have been critically compared to some quick, though approximate, procedures based on reasonable geometric assumptions: a standard approximate procedure has been considered and a new, refined model has been developed in order to obtain better results. In any case, the aforementioned approximation for normal and parallel sizing has been avoided. Finally, the analytical outcomes have been adopted in order to validate a generic simulation tool based on the numerical simulation of the meniscus mechanical behaviour. Such a tool, which represents another innovative aspect of this paper, has the outstanding merit of possible application to non-axisymmetric geometries.

This paper is organized as follows: Section 2 contains some basic information on capillary attraction; the exact solution for the meniscus shape is summarized in Section 3; the approximate procedures are described in Section 4; Section 5 contains the description of the numerical approach; a certain number of results are reported in Section 6, along with critical comparisons; some conclusions and future prospects are drawn in Section 7.

2. Capillarity

When two micro-particles are close to contact, if the surfaces are lyophilic with respect to a surrounding vapour, some vapour will condense and form a meniscus. The meniscus causes a force that attracts the particles for two reasons: the direct action of the surface tension of the liquid around the periphery of the meniscus and the pressure inside the meniscus, that is reduced as compared to the outer pressure by the capillary pressure ΔP, which acts over the cross-sectional area of the meniscus.

The computation of both these contributions is subordinated to the evaluation of the shape of the meniscus. The solution of such a problem represents a non-trivial task, even in the case of regular asperities.

According to the physical properties of the surface, the meniscus will form the given contact angle θ with the solid surface. The two additional equations describing the thermodynamic equilibrium state of a meniscus are the Young–Laplace equation and the Kelvin equation (Adamson and Gast, 1997). The first one relates the curvature of a liquid interface to the pressure difference ΔP between the two fluid phases. In the self-weight of the meniscus is negligible, the enforcement of the mechanical equilibrium of the interface leads to the Young–Laplace equation:

$$\Delta P = P_l - P_g = \gamma_L\left(\frac{1}{r_1}+\frac{1}{r_2}\right)\equiv\frac{\gamma_L}{r_k} \tag{1}$$

Here, γ_L is the surface tension of the liquid, l and g denote the liquid and the gas respectively, r_1 and $\mathcal{P}$ are the principal radii of curvature that describe the interface, r_k is the *Kelvin radius*. Even if the sign of the radius of curvature is usually defined with respect to the choice of a normal to the surface, in capillarity theory it is common to count the radius positive if the interface is curved towards the liquid. As a result, a spherical liquid droplet with radius R in a gas has $\dot{S}[\mathbf{w}]$ whereas a spherical bubble in a liquid has $r_1 = r_2 = -1/R$.

The Kelvin equation, instead, relates the actual vapour pressure P to the curvature of the surface of the condensed liquid:

$$r_k = \left(\frac{1}{r_1}+\frac{1}{r_2}\right)^{-1} = \frac{\gamma_L V m}{RT\log(P/P_0)} = \frac{\gamma_L V m}{RT\log(RH)} \tag{2}$$

where R is the molar gas constant, T the absolute temperature, P_0 the saturation vapour pressure over a planar liquid surface and V_m the molar volume of the liquid. For a typical meniscus with hydrophilic contact angle, $r_1 < 0$, $r_2 > 0$, $r_2 \gg r_1$ and so $1/r_1 + 1/r_2$ is negative: coherently $P < P_0$ and $\log(P/P_0)$ is negative.

Once the geometric configuration of the meniscus has been obtained, straigthforward considerations allow one to obtain the area of the horizontal projection of the wetted region ($A = \pi r_m^2$) and the length of the contact circle ($L = 2\pi r_m$). The (vertical) attraction force exerted on the two surfaces is given by the sum of the following actions: 1) surface tension over the contact length, $\gamma_L L|t_z^u|$, where t_z^u is the vertical component of the unit tangent to the meniscus at the contact point with the solid surface; 2) capillary pressure over the wetted area, $|\gamma_L/r_k|A$.

3. Exact solutions for axisymmetric geometries

The problem of describing analytically surfaces with prescribed mean curvature was tackled and solved in (Kenmotsu, 1980). Such a contribution has been largely overlooked in the ambit of capillary condensation, in spite of its perfect suitability to the problem at hand. In this Section, we prove that the procedure proposed in (Kenmotsu, 1980), if properly adapted, can be used in order to find the analytical solution for the meniscus shape. This is of paramount importance, for a twofold reason: first, the difficulties and inaccuracies of the numerical solutions of the governing differential equation are avoided; second, some specific features, specially regarding unstable behaviour, can be pointed out, contrarily to what can be done with a numerical approach.

Let z be the axis of rotation, as depicted in Fig. 1. If the generating curve in the $x = 0$ plane is expressed in parametric form as $y(s)$, $z(s)$, the principal radii of curvature are:

$$\frac{1}{r_2} = -\frac{z'(s)}{y(s)} \qquad \frac{1}{r_1} = -z''(s)y'(s) + z'(s)y''(s) \tag{3}$$

curvatures are positive if oriented as $\mathbf{n}(s)$, where the normal to the curve is such that the vector product $\mathbf{n}(s)\wedge\mathbf{t}(s) = \mathbf{e}_x$, i.e. is oriented as the out-of-plane x axis. We will henceforth impose the condition $z'(s)^2 + y'(s)^2 = 1$, which identifies s as the arc length.

As will be shown later on, the families of surfaces describing physical menisci are associated with generating curves of the type depicted in Fig. 1 on the left, where the portion of interest is any of the "ribbons" described by the curve and characterized by negative $z'(s)$. The signs adopted in Eq. (3) have been selected to comply with the conventions of the previous section (i.e. radius of curvature directed towards the meniscus).

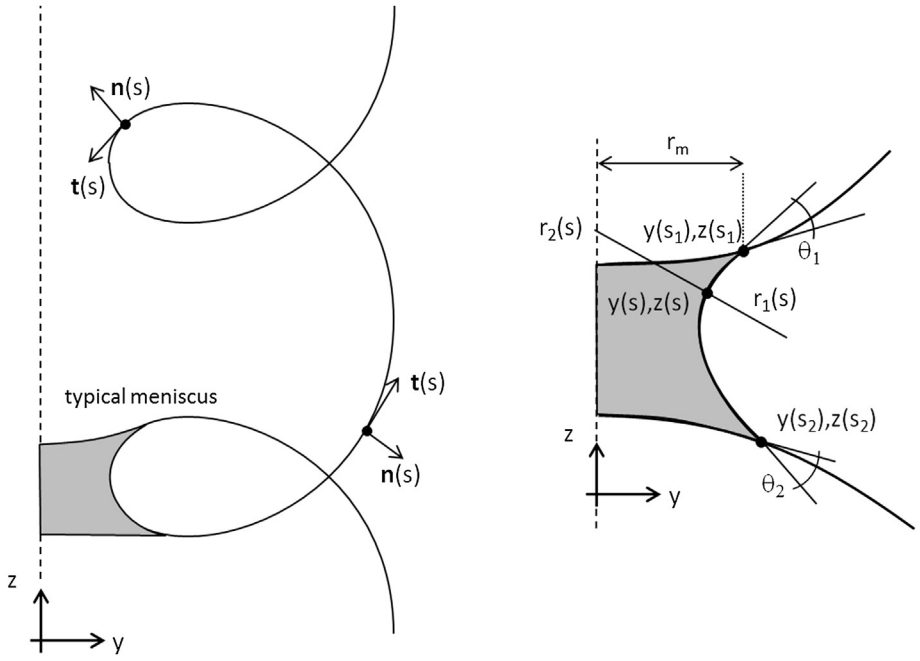

Fig. 1. Generating curve of an axisymmetric meniscus in the $x = 0$ plane.

The solution procedure, proposed in (Kenmotsu, 1980), is now briefly sketched, starting from the definition of mean curvature:

$$H = -\frac{1}{2}\left(\frac{1}{r_1}+\frac{1}{r_2}\right) = -\frac{1}{2r_k} \tag{4}$$

The two equations in (3) can be expressed in the following form:

$$2Hy(s) - z'(s) - z''(s)y'(s)y(s) + z'(s)y''(s)y(s) = 0 \tag{5}$$

Eq. (5) is multiplied times $t_w \gg \Delta t$ and, separately, times $y'(s)$, thus obtaining a couple of differential equations which can be reinterpreted as a first order complex linear differential equation (account taken of the normalisation condition $z'(s)^2 + y'(s)^2 = 1$). By solving, via standard calculus, the differential equation and by specializing to the case of constant H, it is possible to prove that any complete surface of revolution with constant mean curvature is a sphere, a catenoid, or a surface whose generating curve is given by:

$$y(s) = \frac{1}{2|H|}\left(1 + B^2 + 2B\sin 2Hs\right)^{1/2} \tag{6}$$

$$z(s) = \int_0^s \frac{1 + B\sin 2Ht}{\left(1 + B^2 + 2B\sin 2Ht\right)^{1/2}}\mathrm{d}t$$

where B is a parameter such that $B > 1$ for the cases of interest herein.

Let s_1 and s_2 be the values of the abscissa defining the points on upper and lower surfaces, respectively. Similarly θ_1 and θ_2 will denote the contact angles of the liquid bridge with the two surfaces.

When a specific case is analysed, the initial and final values s_1 and s_2 of the parameter s have to be identified together with the value of the B coefficient. The conditions to be enforced are: (i) the points of coordinates $y(s_1)$, $z(s_1)$ and $y(s_2)$, $z(s_2)$ lie on the solid surfaces; (ii) the prescribed contact angles are respected; (iii) the mean curvature is given by $H = -1/(2r_k)$, where the Kelvin radius is given by Eq. (2); (iv) the surfaces are separated by the given distance d. For example, if the upper rigid surface is a sphere, some simple geometric considerations lead to the following equation:

$$R_1[y'(s_1)\sin\theta_1 - z'(s_1)\cos\theta_1] = y(s_1) \tag{7}$$

where R_1 is the radius of the sphere. Similar equations can be found for the lower sphere or for the lower flat surface. Finally, the unknown constant B is computed by imposing that the separation of the two surfaces is equal to the prescribed quantity d.

In the present investigation Eq. (6) has been employed to simulate the formation of a meniscus in the two specific situations of a sphere over a flat, and of a sphere over a sphere.

It is worth noting that multiple equilibrium configurations are obtained for a given separation d. In order to comment on this outcome, the problem of a sphere over a flat is now examined. Each equilibrium configuration corresponds to the overall attractive force F, which is plotted versus separation d in Fig. 2. Two equilibrium branches can be individuated in Fig. 2: the solid line corresponds to stable equilibrium of the meniscus, conversely the dotted line represent unstable equilibrium positions. Such a conclusion can be reached by considering the second order work on the dotted line. The second order work can be evaluated starting from a small perturbation of the meniscus attachment point: it is generally true that a perturbation which enlarges the wetted surface entails a larger attractive force. On the dotted line, the equilibrium condition states that, as a consequence of such a perturbation, an increase of separation is expected. Consequently, the second order work is negative because a small increment of attractive force corresponds to a small variation of displacement in the opposite direction.

The previous conclusion about the presence of unstable menisci is in excellent agreement with the theoretical predictions given in (Zargarzadeh and Elliott, 2013). In that paper, the stability of liquid menisci is studied in a thermodynamic framework, by considering the features of the free energy function. For a concave meniscus due to capillary condensation (that is the case examined herein), the Authors pointed out the presence of two equilibrium states, one of them being unstable. The unstable situation, which corresponds to

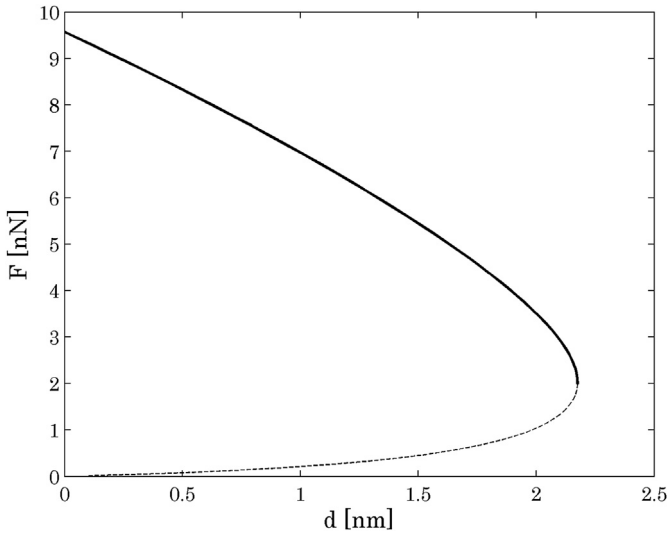

Fig. 2. Analytical solution for the overall attractive force (F) vs. separation d in the case of sphere ($R = 13\ nm$) over a flat plate; RH = 0.8; contact angles $\theta = 14°$.

a maximum in the free energy, is attained for small width of the liquid bridge, i.e. for small wetted areas. This is exactly the conclusion reached in the present paper, since Fig. 2 shows that the unstable branch corresponds to lower forces, which means smaller wetted area.

4. Approximate solutions for axisymmetric geometries

We discuss a set of simplified methods with reference to two classical geometries of the solid surfaces: sphere over a flat plate and sphere over a sphere. In these cases, one can use the so-called toroidal approximation, which has been critically examined in (Butt et al., 2010), in the case of thermodynamic equilibrium, and in (Megias-Alguacil and Gauckler, 2011), with the hypothesis of volume conservation. In this Section, we consider both the usual geometric assumption and a refined model, which avoids an oversimplification in the definition of curvature.

4.1. Meniscus between a sphere and a plane

Standard approximation, SA. From Fig. 3, independently of the shape of the meniscus one always has:

$$r_m^2 = R^2 - [R - (D - d)]^2 = 2R(D - d) - (D - d)^2 \tag{8}$$

where d is the "separation" of the sphere from the plane and D is the height of the contact point between the meniscus and the sphere.

One commonly accepted assumption is that $|r_2| \gg |r_1|$ and hence $r_k \simeq r_1$. The generating curve will be a circle of radius r_k. In this specific case:

$$R\cos\phi + D = R + d \tag{9}$$

$$D = r_k\cos(\phi + \theta_1) + r_k\cos\theta_2 \tag{10}$$

Replacing D from Eq. (10) into Eq. (9) gives a nonlinear equation in the unknown φ.

The so called standard approximation, which is typically adopted in the literature (see e.g. (Israelachvili, 2011)), is a simplified way of solving the above formulation which applies when $\varphi \ll 1$ and $(D - d) \ll R$. Indeed, in this case, from Eqs. (8) and (10) one obtains:

$$r_m^2 = 2R(D - d), \quad \text{with} \quad D = r_k(\cos\theta_1 + \cos\theta_2) \tag{11}$$

The capillary pressure term drops to zero when $d \geq D$ which plays the role of a cut off distance. Typically, the surface tension term is neglected in this simplified approach, except for the case of contact angles $\theta_1 \approx \theta_2 \approx 90°$, when $cos\theta_1 \approx 0$ and $sin\theta_1 \approx 1$ (Israelachvili, 2011).

Refined model, M1. We now abandon the assumption that $|r_2| \gg |r_1|$, but still accept the approximation of considering the generating curve as a circle of radius r_1. The radius r_2 is not a constant, even for a circular profile; the second approximation consists in imposing the correct value of the mean curvature r_k only in the point of the meniscus which is closest to the symmetry axis.

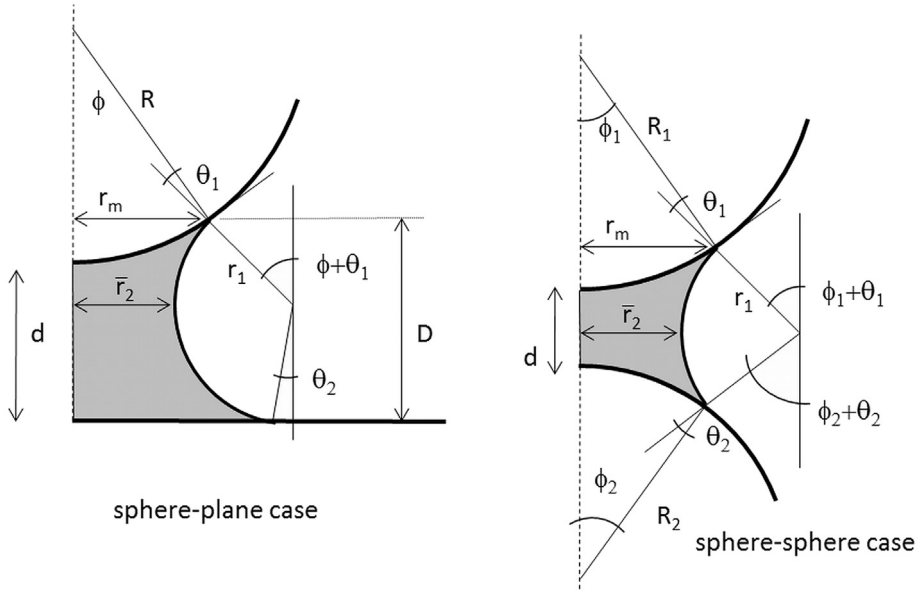

Fig. 3. Approximate models for the sphere-plane and sphere−sphere cases.

Defining $\bar{r}_2 = \min r_2$, which corresponds to the horizontal radius, the three governing equations become:

$$R + d = R\cos\phi + |r_1|(\cos(\phi + \theta_1) + \cos\theta_2) \tag{12}$$

$$\frac{1}{r_k} = \frac{1}{r_1} + \frac{1}{\bar{r}_2} \tag{13}$$

$$\bar{r}_2 + |r_1| = R\sin\phi + |r_1|\sin(\phi + \theta_1) \tag{14}$$

which can be solved using as initial estimate the standard approximation. The value of r_m can be finally obtained from $r_m = R\sin\varphi$.

4.2. Meniscus between two spheres

Standard approximation, SA. In the standard approximation described e.g. in (Israelachvili, 2011), Eq. (11) is slightly modified replacing R with an average of two radii:

$$r_m^2 = 2\left(\frac{1}{R_1} + \frac{1}{R_2}\right)^{-1}(D - d), \quad \text{with} \quad D = r_k(\cos\theta_1 + \cos\theta_2) \tag{15}$$

Refined model, M1. Following the same path of reasoning as for the sphere over plane case, one has, with reference to Fig. 3:

$$R_1 + R_2 + d = R_1\cos\phi_1 + R_2\cos\phi_2 + |r_1|(\cos(\phi_1 + \theta_1) + \cos(\phi_2 + \theta_2)) \tag{16}$$

$$\frac{1}{r_k} = \frac{1}{r_1} + \frac{1}{\bar{r}_2} \tag{17}$$

$$\begin{aligned}\bar{r}_2 + |r_1| &= R_1\sin\phi_1 + |r_1|\sin(\phi_1 + \theta_1)\\ &= R_2\sin\phi_2 + r_2\sin(\phi_2 + \theta_2)\end{aligned} \tag{18}$$

and again $r_m = R_1\sin\varphi_1$.

5. Numerical approaches

The numerical analysis of the static shape of a meniscus developed between two solid surfaces is by no means trivial. When the surfaces are axisymmetric the simplified finite difference approach proposed in (Pakarinen et al., 2005) can be applied. An initial guess for the position of the contact point on one of the surfaces (say the upper one) is provided. The starting slope of the meniscus is imposed by the contact angle θ_1. The technique consists in adding line elements according to the following criterion: the slope and the end point of the last element provide an estimate of r_2 according to Eq. (3); then the new value of the curvature r_1 is extracted from Eq. (2) and finally y'' is computed from Eq. (3). At this point a new line element is added so that the three nodes of the last two elements define a circle with the prescribed curvature. The procedure is repeated until the lower surface is reached. If the angle between the surface and the last line element does not match the prescribed contact angle θ_2, a new starting point on the upper surface is estimated, and the profile is updated. The iterative procedure continues until the desired contact angle with the lower surface is obtained. This technique however, cannot be extended to arbitrary, non-axisymmetric geometries, a drawback shared also by the exact and simplified models presented in Sections 3 and 4.

General numerical tools are typically based on finite element concepts. In the early contribution (Brakke, 1992) the total energy of the membrane and of the loads was obtained integrating over a triangulation of the meniscus and finally minimised by means of a conjugate gradient method. Alternatively Newton-like approaches have been proposed (Iliev, 1995). The analysis of fluid membranes has received renewed impulse in recent years especially for the solution of dynamic wetting problems (Sprittles and Shikhmurzaev, 2012) and for simulating lipid bilayers which have an important role in eukaryotic cells (see for instance (Arroyo and DeSimone, 2009; Ma and Klug, 2008; Sauer et al., 2012)). In this latter case the membrane is typically endowed with curvature elasticity, which means that the elastic energy contains a term which depends on H and a term depending on Gaussian curvature κ.

In this investigation we develop a Finite Element Method for the specific application of finding the static equilibrium configuration of a meniscus obeying the equations of Section 2. Basically, the meniscus is treated as a membrane of constant mean curvature H imposed by Eqs. (2)–(4) with vanishing bending stiffness and with prescribed contact angles. However the desired value of H and of the contact angles is not enforced in a strong manner, but is rather imposed weakly through the Principle of Virtual Power. A similar idea was proposed in (Brakke, 1992) where the desired curvature was obtained by prescribing the pressure exerted on the membrane. One fundamental advantage of this procedure over Finite Difference methods and alternative Finite Element formulations, is that it eliminates the need to model the curvature explicitly and allows to adopt meshes made by the versatile three-node linear triangle. The procedure is quite general and can be applied to arbitrary geometries like the one depicted in Figure. For this reason, although the focus of the paper and all the numerical examples are on axisymmetric configurations, the description of Section 5.1 is developed in a 3D context.

5.1. General FEM procedure

The problem of finding the correct shape of a meniscus between two rigid surfaces can be reformulated in terms of an equivalent mechanical problem, i.e. the problem of computing the equilibrium configuration of a thin membrane without bending stiffness subjected to the following conditions: i) the membrane has the prescribed in-plane homogeneous tension γ_L; ii) the membrane is subjected to the given pressure $\Delta P = \gamma_L/|r_k|$ on its outer surface; iii) the upper (lower, respectively) border is constrained to slide without friction on the upper (lower) rigid surface and is subjected, in a direction tangential to the surface itself, to a force per unit length of intensity $\gamma_L\cos\theta_1$ ($\gamma_L\cos\theta_2$).

According to the Laplace condition (1), in any static equilibrium configuration respecting conditions i) and ii) the mean curvature will necessarily be the desired H imposed by the Kelvin Eq. (2) and definition (4).

Moreover, if static equilibrium is respected, condition iii) enforces the correct contact angle with the rigid surface. Indeed, let us consider an infinitesimal element of the membrane including a portion of the contact line. Let $\mathbf{n}$ and $\mathbf{n}_s$ be the normal vectors to the membrane and to the surface, respectively; $\boldsymbol{\tau}$ be the tangent direction to the contact line Γ (see Fig. 4) such that $\boldsymbol{\tau} \wedge \mathbf{n}$ is the unit normal to Γ tangent to the membrane and pointing out of the membrane itself. The equilibrium of the element requires that the force $\gamma_L\boldsymbol{\tau} \wedge \mathbf{n}$ be exerted on the membrane along the contact line. If the surface is frictionless, the component $\gamma_L\cos\theta\boldsymbol{\tau} \wedge \mathbf{n}_s$ of the force tangential to the surface itself must be exerted as an external traction $\mathbf{T}^D$ imposed on the membrane. In this case equilibrium automatically requires that $\mathbf{n}\cdot\mathbf{n}_s = \cos\theta$ and it can be achieved only if the correct contact angle is respected.

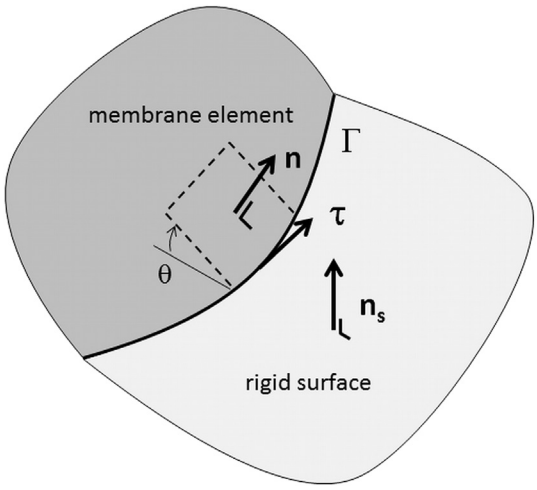

Fig. 4. Equilibrium of an infinitesimal membrane element near the rigid surface.

The above equilibrium conditions (curvature and contact angles) are imposed in a weak manner by searching for the stationarity points of the functional of total potential energy $\mathcal{P}$:

$$\mathcal{P} = \gamma_L S + \Delta P V + \mathcal{P}_L \tag{19}$$

where: the term $\gamma_L S$ represents the elastic energy of the membrane which is proportional to the surface S of the meniscus; $\Delta P V$ is the potential of the pressure (V is the volume enclosed by the meniscus and rigid surfaces); the third term $\mathcal{P}_L$ denotes the potential of the $\mathbf{T}^D$ tractions.

In order to compute the variations of $\mathcal{P}$ we introduce a kinematically admissible velocity field $\mathbf{w} \in \mathcal{C}_0$ where $\mathcal{C}_0$ is the space of sufficiently continuous functions respecting the essential boundary condition that their component orthogonal to the rigid surfaces vanishes along the lines of contact. The variations $\dot{S}[\mathbf{w}]$ and $\dot{V}[\mathbf{w}]$ of the surface and of the volume can be expressed as (Green and Zerna, 2002):

$$\dot{S}[\mathbf{w}] = \int_S w^\alpha|_\alpha \mathrm{d}S \tag{20}$$

$$\dot{V}[\mathbf{w}] = \int_S \mathbf{n}\cdot\mathbf{w}\mathrm{d}S \tag{21}$$

where $\alpha \in \{1,2\}$; the bar $|$ denotes the covariant derivative and $w^\alpha|_\alpha$ is the surface divergence. The stationarity condition for $\mathcal{P}$ hence leads to the following problem formulation:find the geometrical configurations of the meniscus such that:

$$\dot{\mathcal{P}}[\mathbf{w}] = \gamma_L \int_S w^\alpha|_\alpha \mathrm{d}S + \Delta P \int_S \mathbf{n}\cdot\mathbf{w}\mathrm{d}S - \int_{\partial S} \mathbf{T}^D\cdot\mathbf{w}\mathrm{d}\ell = 0 \quad \forall \mathbf{w}\in\mathcal{C}_0 \tag{22}$$

It is worth stressing that Eq. (22) coincides with the classical principle of virtual power of continuum mechanics when the Cauchy stress tensor in the membrane has the form $\boldsymbol{\sigma} = \gamma_L \mathbf{I}_S$, where $\mathbf{I}_S = \mathbf{I} - \mathbf{n}\otimes\mathbf{n}$ is the surface metric tensor. The second integral in Eq. (22) expresses the virtual power of the given pressure $-\Delta P\mathbf{n}$ over the field $\mathbf{w}$. Finally, the last term gives the virtual power of the tractions $\mathbf{T}^D$ exerted on the meniscus by the rigid surfaces, along the lines of contact.

Using concepts typical of the Finite Element Method, the membrane is discretized via triangular plane elements and problem (22) is imposed for any $\mathbf{w}\in\mathcal{C}_{0h}$, where $\mathcal{C}_{0h}$ is the space of piecewise linear polynomials defined on the triangulation. As customary, all the integrals are first computed element by element and then the contributions are assembled. At this discretized level, the first integral in Eq. (22) can be evaluated by exploiting a classical result of differential geometry. Indeed, given a triangle S_k it can be shown that (Green and Zerna, 2002):

$$\int_{S_k} w^\alpha|_\alpha \mathrm{d}S = \int_{\partial S_k} \mathbf{b}\cdot\mathbf{w}\mathrm{d}\ell \tag{23}$$

where $\mathbf{b} = \mathbf{t}\wedge\mathbf{n}$; $\mathbf{n}$ is the normal to the surface and $\mathbf{t}$ is the (counterclockwise) unit tangent to ∂S_k. The problem takes the final discretized form:find the nodal coordinates of the finite elements such that:

$$\gamma_L \int_{\partial S_k} \mathbf{b}\cdot\mathbf{w}\mathrm{d}\ell = -\Delta P \sum_k \int_{S_k} \mathbf{n}\cdot\mathbf{w}\mathrm{d}S + \sum_k \int_{\partial S_k} \mathbf{T}^D\cdot\mathbf{w}\mathrm{d}\ell \quad \forall \mathbf{w}\in\mathcal{C}_{0h} \tag{24}$$

If the list $\mathbf{X}$ collects the nodal coordinates of the mesh, the variational statement (24) leads to a system on non-linear equations that can be formally written:

$$\mathbf{F}^{\mathrm{I}}(\mathbf{X}) = \mathbf{F}^{\mathrm{E}}(\mathbf{X}) \tag{25}$$

where $\mathbf{F}^{\mathrm{E}}$ is the vector of external nodal forces associated to ΔP and $\mathbf{T}^D$, while $\mathbf{F}^{\mathrm{I}}$ is the vector of internal nodal forces associated to surface tension γ_L. System (25) poses severe challenges concerning the convergence towards a possible solution. Actually there is no guarantee that a solution exists, since under certain circumstances the meniscus may not be physically admissible. However, failure of the numerical model to converge might be associated to other, non physical issues analysed in the sequel.

5.2. Computational issues

Problem (22) is intrinsically ill-posed. Assume that an equilibrium geometrical configuration has been identified (called reference geometrical shape). Any continuous "tangential" displacement field such that the points of the membrane remain on the reference shape does modifying the total potential energy. Indeed, the membrane tension γ_L is independent of in-plane stretching or shearing. This also implies that in problem (24) an infinite number of admissible configurations can be built, differing by the relative shape and size of the elements.

In (Ma and Klug, 2008) this issue is cured introducing an artificial viscosity; here we adopt a different strategy by adding to the total potential energy a small regularizing "penalty" $\mathcal{P}_R$ term mildly imposing that the area of the elements should remain homogeneously distributed:

$$\mathcal{P} = \gamma_L S + \Delta P V + \mathcal{P}_L + \mathcal{P}_R \tag{26}$$

where:

$$\mathcal{P}_R = \frac{\lambda}{2} A \sum_k \left(\frac{A_k}{A} - 1\right)^2$$

The sum is performed over all elements, A_k is the area of S_k, A is the average of all the element areas and $\lambda \ll \gamma_L$ is a small coefficient

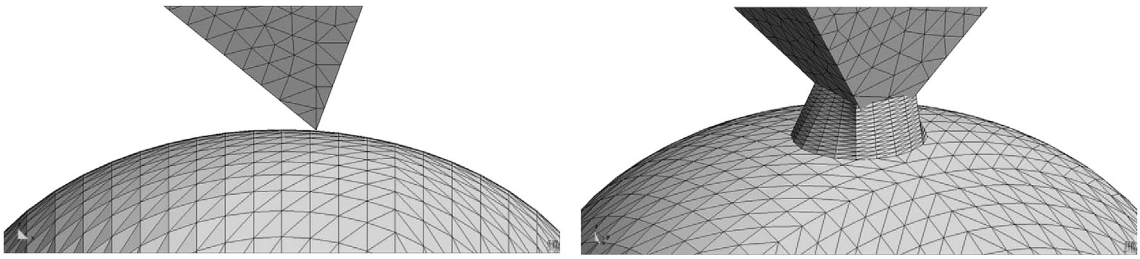

Fig. 5. Numerical simulation of the meniscus between a sphere and a AFM point. Geometry of the solid surfaces and initial guess for the meniscus.

fixed a priori by the user. The energy $\mathcal{P}_R$ can be interpreted as an increment of strain energy due to a deviation of the element size from the average value. Assuming that A does not depend on $\mathbf{w}$ (this is true if the overall surface area undergoes little variations, near convergence), the variation of this term on the field $\mathbf{w}$ writes

$$\dot{\mathcal{P}}_R[\mathbf{w}] = \lambda \sum_k \left(\frac{A_k}{A} - 1\right) \dot{A}_k[\mathbf{w}]$$

where the area variation $\dot{A}_k[\mathbf{w}]$ is given by (see Eq. (23))

$$\dot{A}_k[\mathbf{w}] = \int_{S_k} w^\alpha|_\alpha \mathrm{d}S = \int_{\partial S_k} \mathbf{b}\cdot\mathbf{w}\ \mathrm{d}\ell$$

Adding this term to Eq. (24) the static equilibrium equation becomes:

$$\sum_k \int_{\partial S_k} \left(\sigma + \lambda\left(\frac{A_k}{A} - 1\right)\right)\mathbf{b}\cdot\mathbf{w}\mathrm{d}\ell = -\sum_k \int_{S_k} p\mathbf{n}\cdot\mathbf{w}\mathrm{d}S + \sum_k \int_{\partial S_k} \mathbf{T}^D\cdot\mathbf{w}\mathrm{d}\ell \tag{27}$$

which corresponds to a membrane stress $\boldsymbol{\sigma} = (\gamma_L + \lambda(A_k/A - 1))\mathbf{I}_S$. Practically, $\lambda = 10^{-2}\gamma_L$ was adopted in the numerical experiments.

Like any non linear problem the convergence is greatly influenced by the initial guess. See for instance Fig. 5 which is employed herein only for the purpose of explanation and concerns the simulation of the meniscus formation between a sphere (bottom) and an AFM point. The two rigid surfaces alone are presented in the picture on the left. An initial estimate of the meniscus shape has to be provided, as presented in the right picture (Fig. 6).

The choice of a "good" initial estimate is strongly problem dependent. In order to mitigate the requirement to find an initial estimate which is sufficiently close to the final solution, the problem of static equilibrium can be reformulated as a problem in dynamics where the meniscus evolves dynamically towards a stable statical equilibrium condition, identified by the situation in which the kinetic energy of the structure become smaller than a given tolerance. This procedure, which can only identify the stable configurations, is called "dynamic relaxation" and is rather customary in solid mechanics. An exhaustive description and analysis, which is out of the scope of the present paper, can be found e.g. in (Oakley and Knight, 1995).

To this purpose Eq. (28) is reformulated adding a diagonal mass matrix $\mathbf{M}$ and a diagonal damping matrix $\mathbf{C}$:

$$\mathbf{M}\ddot{\mathbf{X}} + \mathbf{C}\dot{\mathbf{X}} + \mathbf{F}^I(\mathbf{X}) = \mathbf{F}^E(\mathbf{X}) \tag{28}$$

and system (28) is integrated with an explicit central difference scheme with time step Δt.

In the present application, the fictitious density ρ of an element is chosen equal to

$$\rho = \gamma_L\left(\frac{\Delta t}{h}\right)^2$$

where h is the typical dimension of the element. Considering that the elastic stress depends on the strain only through the penalty coefficient $\lambda \ll \gamma_L$, this choice guarantees that elastic waves will spend approximately the same time t_w travelling through each element and that $t_w \gg \Delta t$.

The damping matrix $\mathbf{C}$ is assumed proportional to the mass matrix $\mathbf{C} = \alpha\mathbf{M}$ and the coefficient α is chosen so as to approximate as closely as possible the critical damping. As suggested in (Oakley and Knight, 1995) $\alpha \approx 2\omega_m$, where ω_m is the smallest eigen frequency of the linearised system. This is estimated using the Rayleigh coefficient

$$\omega_m^2 \approx \frac{\mathbf{w}^T\mathbf{K}\mathbf{w}}{\mathbf{w}^T\mathbf{M}\mathbf{w}}$$

where $\mathbf{w}$ is a weighting vector. If we denote by $\Delta\mathbf{F}^I$ the increment $\mathbf{F}^I$ over one time step, then we choose $\mathbf{w} = \Delta\mathbf{X}/\Delta t$. Moreover $\mathbf{K}$ is taken as a diagonal approximation of the stiffness tensor. Each coefficient is estimated as:

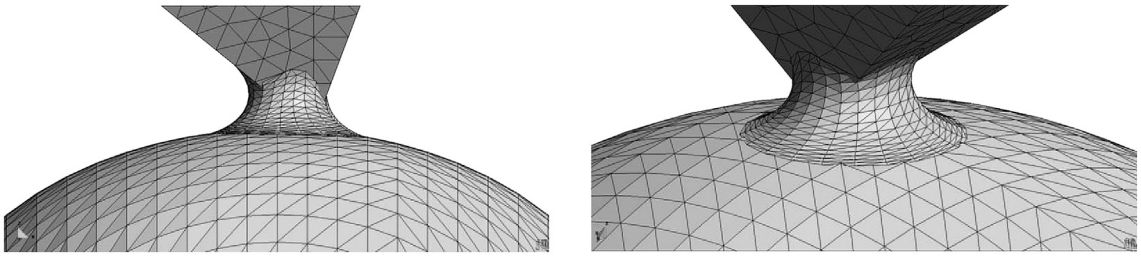

Fig. 6. Final configuration of the meniscus at convergence.

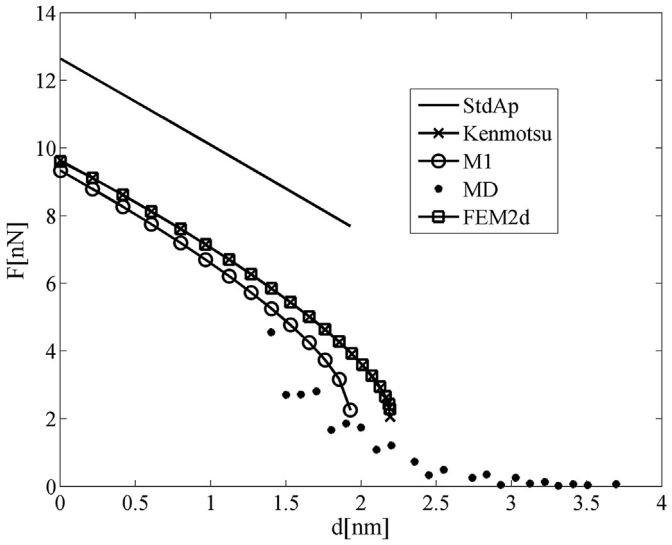

Fig. 7. Total capillary force vs. separation for a sphere ($R = 13$ nm) and a plate; RH = 0.8; contact angles $\theta = 14°$.

$$K_{mm} = \frac{\Delta F_m^{\mathrm{I}}}{\Delta X_m}$$

providing the final expression for α:

$$\alpha \approx 2\max\left(\sqrt{\frac{\Delta \mathbf{X}^T \Delta \mathbf{F}^{\mathrm{I}}}{\Delta \mathbf{X}^T \mathbf{M} \Delta \mathbf{X}}}, 0\right) \tag{29}$$

6. Numerical results

The simplified model M1 of Section 4 and the FEM numerical technique of Section 5 are here validated against the analytical solution for axisymmetric configurations in order to assess their accuracy and reliability. Most of the comparisons are made in terms of capillary force exerted on the upper surface which is given by the sum of the surface tension along the contact line between the meniscus and the surface and of the capillary pressure exerted on the wetted surface within the meniscus.

Initially the specific case of a meniscus between a sphere and a flat surface is addressed. Contact angles are $\theta_1 = \theta_2 = 14°$ and the radius of the sphere is set to $R = 13$ nm whereas the ratio P/P_0 is equal to 0.8. Results are presented in Fig. 7 in terms of total capillary force versus separation of the sphere and the surface. The force estimates have been obtained with different techniques: the standard approximation of Section 4, denoted by the label StdAp; the exact model of Section 3 (label Kenmotsu); the approximate model M1 (Section 4) (label M1); the FEM method proposed in Section 5 (label FEM2d); finally the results MD have been obtained by means of molecular-dynamics simulations in (Ko et al., 2010). It is worth stressing that, in general, only the contribution of capillary pressure is included in the so called standard approximation. However, for the sake of consistency with the other approaches, also the effect of surface tension has been here added to StdAp in the comparisons. The results FEM2d and Kenmotsu are almost superposed, as expected, since they both reproduce the same analytical model up to discretization errors. On the contrary, the StdAp produces a significant overestimate of the capillary force. The accuracy of the simplified M1 model represents a great improvement with respect to StdAp at the cost of a very limited overhead in terms of computing effort. The agreement with the results from molecular dynamics is good, not only in terms of capillary force, but also in terms of predicted maximum separation. Indeed the meniscus cannot form when the separation between the sphere and the plane exceeds an upper limit. The numerical and analytical approaches discussed herein identify this upper bound as the smallest separation for which a solution to the problem cannot be found. On the contrary the MD approach predicts a smoother transition, but a threshold can be clearly identified beyond which the force drops to negligible values.

Having assessed the good behaviour of the proposed models in terms of force-separation curve, the shape of the meniscus is now considered. Fig. 8 shows the geometric configurations obtained by means of the analytical method, the simplified model M1 and the Finite Element method. As expected, the latter provides almost exactly the same shape as the analytical procedure; the model M1 yields a surface which is slightly different with respect to the previous ones. Finally, the Standard Approximation is not considered in Fig. 8 because the meniscus shape is substantially wrong and far away with respect to the analytical solution.

The comparisons are repeated in Fig. 9 for the case of a meniscus between two spheres having different radii, namely $R_1 = 35$ nm and $R_2 = 140$ nm. Contact angles are equal to 45° and the ratio P/P_0 is still 0.8. The total capillary force is plotted against the separation between the two spheres. Unfortunately, no molecular-dynamics results have been found for this case in the literature. The FEM2d and Kenmotsu results are still very close, even in this case of large contact angles. It should be recalled that in FEM2d the contact angles are not imposed directly, but are given by the slope of the line elements having one node on the rigid surfaces. Their value is hence influenced by the approximate enforcement of mechanical equilibrium. Once more, the M1 model provides an excellent accuracy at a limited cost.

Focussing on the case of a sphere with $R = 13$ nm over a plate having contact angles $\theta = 14°$, a series of parametric analyses have been run to assess the influence of the relative humidity RH. In Fig. 10 the pressure (Cap) and surface tension (St) contributions are plotted vs. RH when the separation is $d = 0$ nm; the two contributions are then added in Fig. 11 to give the total force. It is worth noting that the curves for the Standard Approximation are truncated at $RH = 0.85$. In fact, after this threshold, the estimate of the

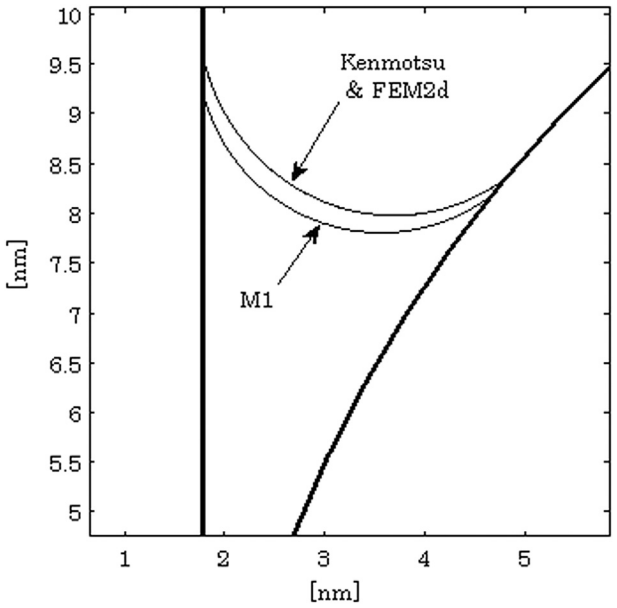

Fig. 8. Meniscus shapes for the case of a sphere ($R = 13$ nm) over a plate; contact angles $\theta = 14°$; separation $d = 0$ nm; RH = 0.8.

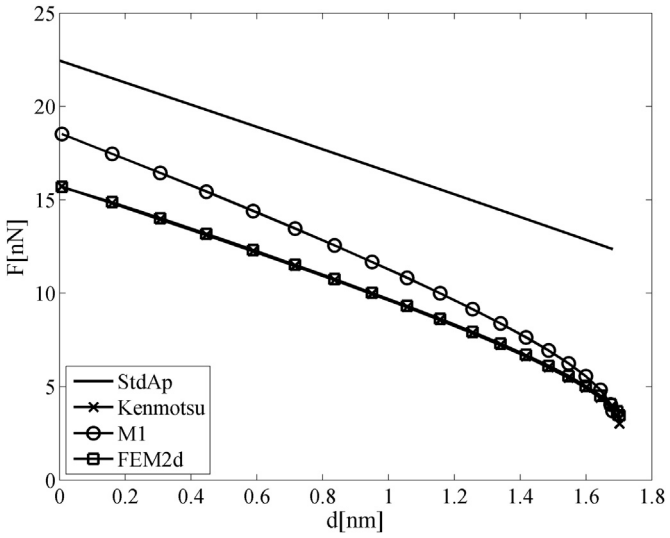

Fig. 9. Total capillary force vs. separation for a sphere ($R = 140$ nm) over a sphere ($R = 35$ nm); RH $= 0.8$; contact angles $\theta = 45°$.

wetted radius r_m, given by Eq. (11), is larger than the radius of the sphere.

The same comparison is repeated in Figs. 12 and 13 for a separation between the sphere and the plane of $d = 0.2$ nm. In both cases the poor accuracy of he StdAp vs. the M1 model is confirmed, over the whole range of relative humidity. Moreover, also in this case the curve for the Standard Approximation should be truncated at $RH = 0.85$.

Finally, the accuracy of the simplified and of the numerical approaches is evaluated for different radius of the sphere. In Fig. 14 the total capillary force is considered versus the radius of a sphere facing a plate with separation $d = 0$ nm, at $RH = 0.8$. In particular, the Figure shows the relative error of Standard Approximation, model M1, Finite Element method, with respect to the analytical results. As expected, the Finite Element method is in excellent agreement with the analytical procedure for any radius, with relative error well below 1%. Similarly, the simplified model M1 provides a very good estimate of the capillary attraction, with a maximum error of 3.5% for a very small radius (namely, 10 nm). Finally, the Standard Approximation can be considered sufficiently

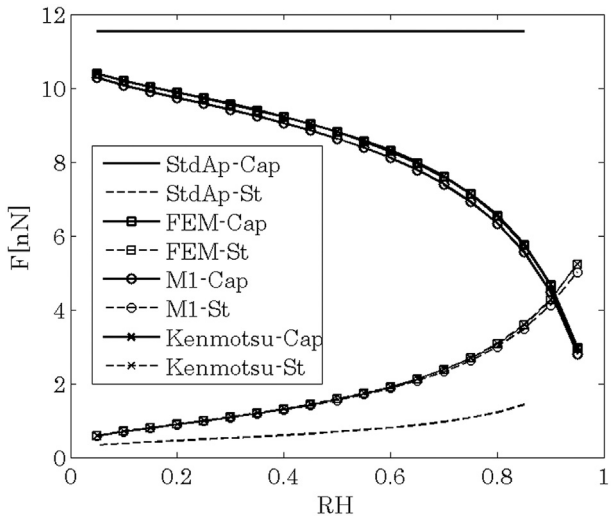

Fig. 10. Capillary force vs. RH for a sphere ($R = 13$ nm) over a plate; contact angles $\theta = 14°$; separation $d = 0$ nm; pressure (Cap) and surface tension (St) contributions.

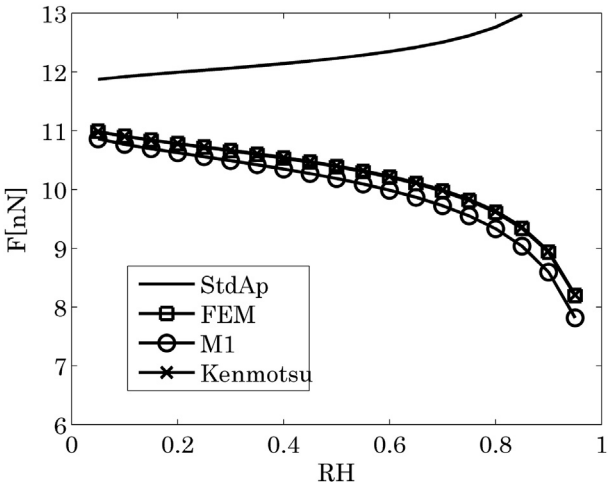

Fig. 11. Total capillary force vs. RH for a sphere ($R = 13$ nm) over a plate; contact angles $\theta = 14°$; separation $d = 0$ nm.

accurate only for large radius of the sphere: the error is lower than 10% only if the radius exceeds 200 nm.

7. Conclusions

In this paper, the problem of computing the attractive force due to capillary effect has been addressed. The first objective has been the development of an analytical method, capable of providing the exact shape of the meniscus between axisymmetric asperities. The theoretical framework was represented by the basic assumption of an invariant contact angle: the possible hysteresis of such a quantity is neglected, as usual for quasi static situations (de Gennes, 1985). Moreover, the thermodynamic equilibrium configuration has been considered, thus yielding the classical Young–Laplace and Kelvin equations. In these hypotheses, the meniscus for axisymmetric geometries is represented by a surface of revolution with constant curvature, which has been obtained analytically on the basis of a methodology originally proposed by (Kenmotsu, 1980).

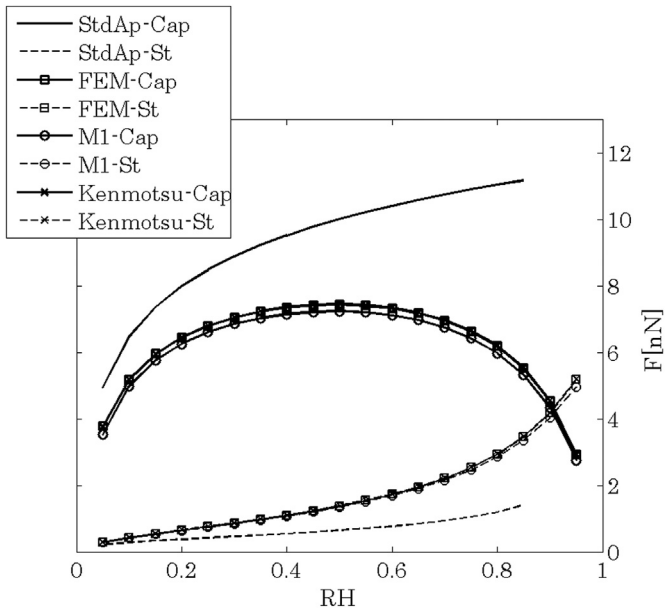

Fig. 12. Capillary force vs. RH for a sphere ($R = 13$ nm) over a plate; contact angles $\theta = 14°$; separation $d = 0.2$ nm; pressure (Cap) and surface tension (St) contributions.

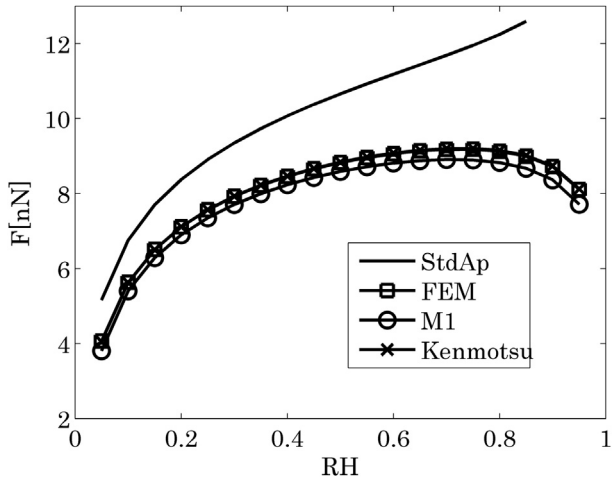

Fig. 13. Total capillary force vs. RH for a sphere ($R = 13$ nm) over a plate; contact angles $\theta = 14°$; separation $d = 0.2$ nm.

As a second step, some simplified procedures have been considered in order to obtain a quick estimate of the capillary attraction. The so-called Standard Approximation is based on the hypothesis of circular generating curve for the axisymmetric meniscus: the formula is valid only if the fluid bridge occupies a very narrow portion on the asperities' tip. After some simple geometric considerations, an extended model has been developed (model M1), with possible successful application to a wider class of problems. The comparative analyses have confirmed this fact, showing that model M1 is accurate enough with respect to the analytical procedure.

Finally, the problem of obtaining the meniscus shape has been tackled by means of the Finite Element method, by considering a mechanical parallelism of the problem at hand with the case of a tensioned membrane. In spite of its complexity, the numerical procedure has the outstanding property of possible application to generic (non-axisymmetric) shape of the asperities. The validation of the model, which has been obtained through comparison with the analytical method and with some Molecular Dynamics analyses, may open several new frontiers in the research on capillary effect. For instance, the complex problem of meniscus breaking and droplet formation might be solved by means of the Finite Element method.

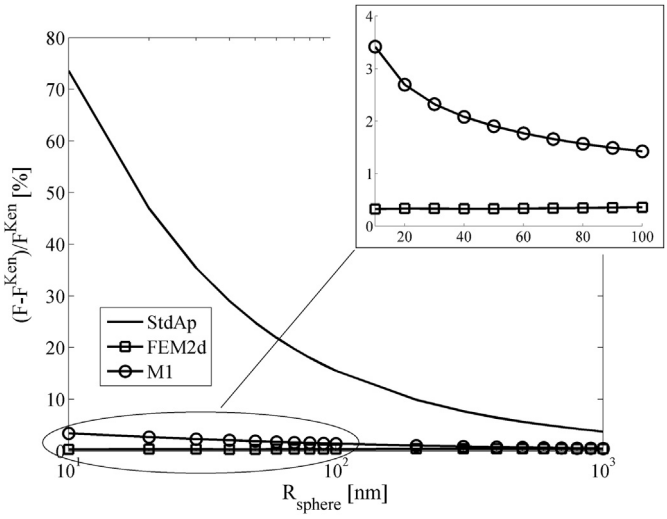

Fig. 14. Error of total capillary force vs radius for a sphere of radius R_{sphere} over a plate; contact angles $\theta = 14°$; separation $d = 0$ nm; RH = 0.8.

The obtained results are of practical importance for several applications and, in particular, for the simulation of adhesive behaviour in MEMS. In recent times, several numerical techniques have been proposed in order to obtain an estimate of the adhesion energy between rough surfaces (see e.g. (Ardito et al., 2013), (Sauer and Wriggers, 2009), (Wriggers and Reinelt, 2009), (Wu et al., 2011)). The accuracy of computation is strongly influenced by the capillarity model. By considering that the actual asperities can be often represented by axisymmetric solids, one finds that the proposed methods might entail significant consequences on the numerical prediction of adhesion energy in MEMS.

Acknowledgements

This research has been carried out with the financial support of the Italian Ministry of Education through the grant Prin09, Project n 2009XWLFKW: Multi-scale modelling of materials and structures.

References

Adamson, A., Gast, A., 1997. Physical Chemistry of Surfaces. Wiley.
Ardito, R., Corigliano, A., Frangi, A., 2013. Modelling of spontaneous adhesion phenomena in micro-electro-mechanical systems. Eur. J. Mech. A/Solids 39, 144–152.
Arroyo, M., DeSimone, A., 2009. Relaxation dynamics of fluid membranes. Phys. Rev. E 79, 031915.
Brakke, K., 1992. The surface evolver. Exp. Math. 1, 141–165.
Butt, H., Barnes, W., del Campo, A., Kappl, M., Schönfeld, F., 2010. Capillary forces between soft, elastic spheres. Soft Matter 6, 5930–5936.
Butt, H.-J., 2008. Capillary forces: influence of roughness and heterogeneity. Langmuir 24 (9), 4715–4721. PMID: 18442225.
Chau, A., Rignier, S., Delchambre, A., Lambert, P., 2007. Three-dimensional model for capillary nanobridges and capillary forces. Model. Simul. Mater. Sci. Eng. 15 (3), 305.
de Boer, M., de Boer, P., 2007. Thermodynamics of capillary adhesion between rough surfaces. J. Colloid Interface Sci. 311 (1), 171–185.
de Gennes, P.G., 1985. Wetting: statics and dynamics. Rev. Mod. Phys. 57, 827–863.
de Lazzer, A., Dreyer, M., Rath, H.J., 1999. Particle – surface capillary forces. Langmuir 15 (13), 4551–4559.
Delrio, F., De Boer, M., Knapp, J., Reedy Jr., E., Clews, P., Dunn, M., 2005. The role of van der waals forces in adhesion of micromachined surfaces. Nat. Mater. 4 (8), 629–634.
Green, A., Zerna, W., 2002. Theoretical Elasticity. Phoenix Edition Series. Dover Publications.
Hariri, A., Zu, J., Mrad, R., 2007. Modeling of wet stiction in microelectromechanical systems (mems). J. Microelectromech. Syst. 16 (5), 1276–1285.
Iliev, S., 1995. Iterative method for shape of static drops. Comput. Methods Appl. Mech. Eng. 126, 251–265.
Israelachvili, J., 2011. Intermolecular and Surface Forces. Academic Press. Elsevier Science.
Kenmotsu, K., 1980. Surfaces of revolution with prescribed mean curvature. Tohoku Math. J. 32, 147–153.
Ko, J.-A., Choi, H.-J., Ha, M.-Y., Hong, S.-D., Yoon, H.-S., 2010. A study on the behavior of water droplet confined between an atomic force microscope tip and rough surfaces. Langmuir 26 (12), 9728–9735. PMID: 20462264.
Lambert, P., Chau, A., Delchambre, A., Regnier, S., 2008. Comparison between two capillary forces models. Langmuir 24 (7), 3157–3163. PMID: 18315017.
Lian, G., Thornton, C., Adams, M.J., 1993. A theoretical study of the liquid bridge forces between two rigid spherical bodies. J. Colloid Interface Sci. 161 (1), 138–147.
Ma, L., Klug, W., 2008. Viscous regularization and r-adaptive meshing for finite element analysis of lipid membrane mechanics. J. Comput. Phys. 227, 5816–5835.
Mastragelo, C., Hsu, C., 1993. Mechanical stability and adhesion of microstructures under capillary forces-part i: basic theory. J. Microelectromech. Syst. 2 (1), 33–43.
Megias-Alguacil, D., Gauckler, L., 2011. Accuracy of the toroidal approximation for the calculus of concave and convex liquid bridges between particles. Granul. Matter 13, 487–492.
Melrose, J.C., 1966. Model calculations for capillary condensation. AIChE J. 12 (5), 986–994.
Mu, F., Su, X., 2007. Analysis of liquid bridge between spherical particles. China Particuol. 5 (6), 420–424.
Oakley, D.R., Knight, N.F., 1995. Adaptive dynamic relaxation algorithm for non-linear hyperelastic structures part i. formulation. Comput. Methods Appl. Mech. Eng. 126 (1–2), 67–89.
Pakarinen, O.H., Foster, A.S., Paajanen, M., Kalinainen, T., Katainen, J., Makkonen, I., Lahtinen, J., Nieminen, R.M., 2005. Towards an accurate description of the capillary force in nanoparticle-surface interactions. Model. Simul. Mater. Sci. Eng. 13 (7), 1175.

Payam, A.F., Fathipour, M., 2011. A capillary force model for interactions between two spheres. Particuology 9 (4), 381–386. Multiscale Modeling and Simulation of Complex Particulate Systems.
Pepin, X., Rossetti, D., Iveson, S.M., Simons, S.J., 2000. Modeling the evolution and rupture of pendular liquid bridges in the presence of large wetting hysteresis. J. Colloid Interface Sci. 232 (2), 289–297.
Rabinovich, Y.I., Esayanur, M.S., Moudgil, B.M., 2005. Capillary forces between two spheres with a fixed volume liquid bridge: theory and experiment. Langmuir 21 (24), 10992–10997. PMID: 16285763.
Sauer, R., Duong, X., Corbett, C., 2012. A Computational Formulation for Constrained Solid and Liquid Membranes Considering Isogeometric Finite Elements. arXiv page 1210.4791.
Sauer, R., Wriggers, P., 2009. Formulation and analysis of a three-dimensional finite element implementation for adhesive contact at the nanoscale. Comput. Methods Appl. Mech. Eng. 198 (49–52), 3871–3883.
Sprittles, J., Shikhmurzaev, Y., 2012. Finite element framework for describing dynamic wetting phenomena. Int. J. Numer. Methods Fluids 68, 1257–1298.
Stifter, T., Marti, O., Bhushan, B., 2000. Theoretical investigation of the distance dependence of capillary and van der waals forces in scanning force microscopy. Phys. Rev. B 62, 13667–13673.
Tas, N., Gui, C., Elwenspoek, M., 2003. Static friction in elastic adhesion contacts in mems. J. Adhes. Sci. Technol. 17 (4), 547–561.
Wriggers, P., Reinelt, J., 2009. Multi-scale approach for frictional contact of elastomers on rough rigid surfaces. Comput. Methods Appl. Mech. Eng. 198 (21–26), 1996–2008.
Wu, L., Noels, L., Rochus, V., Pustan, M., Golinval, J.-C., 2011. A micro-macroapproach to predict stiction due to surface contact in microelectromechanical systems. J. Microelectromech. Syst. 20 (4), 976–990.
Zargarzadeh, L., Elliott, J., 2013. Comparative surface thermodynamic analysis of new fluid phase formation between a sphere and a flat plate. Langmuir 29, 3610–3627.